Geomorphology 105 (2009) 239–252

Contents lists available at ScienceDirect

Geomorphology

journal homepage: www.elsevier.com/locate/geomorph

Spatial patterns of old, deep-seated landslides: A case-study in the northern Ethiopian highlands

M. Van Den Eeckhaut [a,b,*], J. Moeyersons [c], J. Nyssen [d], Amanuel Abraha [e], J. Poesen [a], Mitiku Haile [e], J. Deckers [f]

[a] Physical and Regional Geography Research Group, K.U. Leuven, Celestijnenlaan 200 E, B-3001 Heverlee, Belgium
[b] Research Foundation-Flanders, Belgium
[c] Royal Museum for Central Africa, B-3080 Tervuren, Belgium
[d] Department of Geography, Ghent University, B-9000 Ghent, Belgium
[e] Mekelle University, Mekelle, Ethiopia
[f] Institute for Land and Water Management, K.U. Leuven, B-3001 Heverlee, Belgium

ARTICLE INFO

Article history:
Received 17 March 2008
Received in revised form 24 September 2008
Accepted 29 September 2008
Available online 25 October 2008

Keywords:
Ethiopian highlands
Landslide susceptibility
Weights of evidence
Spatial validation

ABSTRACT

During the last decade, slope failures were reported in a 500 km^2 study area in the Geba–Werei catchment, northern Ethiopia, a region where landslides were not considered an important hazard before. Field observations, however, revealed that many of the failures were actually reactivations of old deep-seated landslides after land use changes. Therefore, this study was conducted (1) to explore the importance of environmental factors controlling landslide occurrence and (2) to estimate future landslide susceptibility. A landslide inventory map of the study area derived from aerial photograph interpretation and field checks shows the location of 57 landslides and six zones with multiple landslides, mainly complex slides and debris flows. In total 14.8% of the area is affected by an old landslide. For the landslide susceptibility modelling, weights of evidence (WofE), was applied and five different models were produced. After comparison of the models and spatial validation using Receiver Operating Characteristic curves and Kappa values, a model combining data on elevation, hillslope gradient, aspect, geology and distance to faults was selected. This model confirmed our hypothesis that deep-seated landslides are located on hillslopes with a moderate slope gradient (i.e. 5°–13°). The depletion areas are expected on and along the border of plateaus where weathered basalts rich in smectite clays are found, and the landslide debris is expected to accumulate on the Amba Aradam sandstone and upper Antalo limestone. As future landslides are believed to occur on inherently unstable hillslopes similar to those where deep-seated landslides occurred, the classified landslide susceptibility map allows delineating zones where human interventions decreasing slope stability might cause slope failures. The results obtained demonstrate that the applied methodology could be used in similar areas where information on the location of landslides is essential for present-day hazard analysis.

1. Introduction

Although landslides on the African continent have considerable social and economic consequences (e.g. Ngecu and Ichang'I, 1999; Ayonghe et al., 2004), and although they are important for the development of hillslopes (e.g. Ayalew and Yamagishi, 2004; Knapen et al., 2006) information on this geomorphic process is far more restricted compared to other continents. A study on the global occurrence of fatal landslides in 2007 by Petley (2008) reports only 13 of 395 fatal landslides to have occurred in Africa, but the low number is followed by a comment suggesting that a number of fatal landslide events might be missed, especially when they occurred in remote places or where they are reported in a local language. This comment suggests that also a review by Alcántara-Ayala (2002) probably underestimates the number of landslide events on the African continent.

Aware of the lack of information on landslides in Africa, several studies have tried to catch up with the rest of the world during the last decades (e.g. Temple and Rapp, 1972; Moeyersons, 1981, 1989, 2001, 2003; Garland and Olivier, 1993; Davies, 1996; Ayonghe et al., 1999, 2004; Ngecu and Ichang'I, 1999; Ngecu and Mathu, 1999; Bell and Maud, 2000; Ibe and Ebe, 2000; Temesgen et al., 2001; Nyssen et al., 2003; Moeyersons et al., 2004, 2008; Ngecu et al., 2004; Knapen et al., 2006; Claessens et al., 2007; Zogning et al., 2007). With the exception of the paper by Claessens et al. (2007) all these studies present case-studies of fatal and destructive landslides, descriptive analyses of the causal factors and consequences, or statistical analyses of rainfall

* Corresponding author. Physical and Regional Geography Research Group, K.U. Leuven, Celestijnenlaan 200 E, B-3001 Heverlee, Belgium. Tel.: +32 16 32 64 17; fax: +32 16 32 39 80.
E-mail address: Miet.vandeneeckhaut@ees.kuleuven.be (M. Van Den Eeckhaut).

0169-555X/$ – see front matter © 2008 Elsevier B.V. All rights reserved.
doi:10.1016/j.geomorph.2008.09.027

events that triggered landslides. These studies often have a high local importance, as they contribute to better understanding of the site-specific problems. On a larger scale however these studies have only limited value.

Claessens et al. (2007) presented a physical deterministic slope stability model, tested in a Ugandan study area, for assessment of landslide susceptibility. Landslide susceptibility maps portray the propensity of a site to generate landslides (Guzzetti et al., 2006). Regional-scale susceptibility maps can be created with a variety of methods. Carrara et al. (1995), Soeters and van Westen (1996), Guzzetti et al. (1999) and others provide clear syntheses, and distinguish among geomorphological, heuristic, statistical and physically-based models. In regions with limited data-availability, spatially distributed physically-based or deterministic models generating objective, site-specific factors of safety (e.g. Frattini et al., 2004), failure probabilities (e.g. van Westen et al., 1993) or critical rainfall (e.g. Claessens et al., 2007) have two important limitations. They require detailed geotechnical data, which is often absent or only available for point locations, and the most commonly used models (e.g. infinite slope model) are too simplistic for most landslide types (Guzzetti et al., 1999). The lack of detailed geotechnical data might be a reason why Temesgen et al. (2001) adopted a heuristic or expert-based approach in which weights, attributed to classes of different environmental factors, were added to obtain a landslide susceptibility map for a study area in the eastern margin of the Main Ethiopian rift.

The objective of this study is to present a landslide susceptibility model (1) that helps in understanding the spatial distribution of landslides, (2) that is objective and can be validated, (3) that combines weights attributed to the classes of environmental factors, and (4) that allows regional analyses in remote areas where detailed large-scale data is not available. More specifically, the statistical model, weights of evidence (WofE), will be used to estimate landslide susceptibility and to explore the influence of environmental characteristics on slope failure. Similar to all other statistical models, WofE require a detailed landslide inventory, because the approach is based on the assumption that future landslides will occur under the same conditions and on sites with similar characteristics as currently affected landslide sites. A detailed inventory of old, deep-seated landslides, created for a representative 500 km^2 study area in the Ethiopian highlands, will be used to meet the objectives. Hence, we will show that WofE not only allows assessing the susceptibility to more recent shallow landslides, but that it also helps in understanding the spatial distribution of these deep-seated landslides.

2. Study area

This study focuses on landslide susceptibility in the northern Ethiopian highlands (Fig. 1). More specifically, a 500 km^2 study area around Hagere Selam (Dogu'a Tembien district, Tigray) was selected. This area, located in the Geba and Werei river catchments, was selected because of the outcrop of a complete geological succession representative for the region and because of the availability of background data as several studies on soil erosion processes and soil conservation have been carried out there (e.g. Nyssen et al., 2000; Gebremichael et al., 2005; Descheemaeker et al., 2006).

The study area covers the north-western part of the Mekelle outlier, which is composed of a nearly horizontal succession of Mesozoic layers consisting of a lower sandstone unit, the Adigrat sandstone, an intermediate large carbonate unit, the Antalo limestone and Agula shale, and an upper sandstone unit, the Amba Aradam Formation (Bosellini et al., 1997; Fig. 2). Two layers of flood basalts of Tertiary age, intercalated with silicified lacustrine deposits (i.e. white silicified clays and marls with abundant cherts; Bosellini et al., 1997; Asrat, 2002), unconformably overlie the Amba Aradam Formation. As a result of contact metamorphism, the top of the Amba Aradam sandstone is resistant and impervious. A network of Mekelle dolerite sills and dykes (Dramis et al., 2002) developed more or less contemporaneously with the plateau basalts. The Imba Degoa Ridge (Figs. 1 and 2) is, for example, a feeder dyke of the Mekelle dolerite sill.

The present-day, structural landscape of tabular, stepped landforms is related to differential erosion of the outcropping monoclinal lithological layers (Nyssen et al., 2004). Harder layers such as the Amba Aradam sandstone and some local banks in the Antalo limestone form clear structural levels (e.g. Fig. 3). Erosion was enhanced by up to 2000 m Miocene and Plio-Pleistocene tectonic uplifts that were related to the Ethiopian rift (Almond, 1986; Bosellini et al., 1997), located ca. 100 km east of the study area. Several faults cross the study area. SE–NW oriented faults are dominant.

The altitude of the study area ranges between 1370 and 2835 m a.s.l. with a dominance of areas with an altitude between 2000 and 2500 m a.s.l (Fig. 1). Slope gradients up to 35° and more can be found in the study area, but ca. 70% of the hillslope sections have slope gradients below 15°. The region has an average annual rainfall depth of 750 mm showing a bimodal distribution with a first minor peak from March to May and a second main peak (i.e. 80% of the annual rainfall) from June to September (Nyssen et al., 2005). Daily air temperature is characterised by large variations (e.g. from 5 °C to 28 °C; Nyssen et al., 2005), but temperatures below 0 °C were never measured over the last decades.

With regard to the soilscape, Vertisols and vertic Cambisols often rich in smectite clays are found in the basalts above the Amba Aradam sandstone. Lower tracts of the valleys on Antalo limestone have Calcisols, other calcaric soils and some Vertisols (Nyssen et al., 2008). Over the last 3000 years large-scale human-induced land use changes from forest to croplands have taken place (Nyssen et al., 2004), causing important water and tillage erosion. In order to reduce soil erosion rates, an active policy of reforestation of the steepest slopes has taken place since 1980s. Nyssen et al. (2003) suggested that increased infiltration on these reforested hillslopes (i.e. exclosures) might locally decrease slope stability.

3. Materials and methods

3.1. Landslide inventory

The presence of landslides in the study area became only clear during the last decade, after reactivation of some old landslides during construction works, such as roadworks east of Hagere Selam, and installation of electricity poles. For the study area, a landslide inventory map was prepared from 1:50,000 aerial photograph interpretation in combination with detailed field checks conducted by four geomorphologists in April and May 2007 (Moeyersons et al., 2008). The landslides were mapped on a digital topographical map, and the landslide depletion (i.e. upper part of landslides with concave plan and profile curvature) and accumulation (i.e. lower part of landslides with convex plan and profile curvature) areas were mapped separately.

During field control, landslides were classified using the classification suggested by Cruden and Varnes (1996). The resulting inventory map (Fig. 1) shows the location of 57 old deep-seated mass movements, mainly complex and rotational slides and debris flows (Fig. 3A–E), and six zones with multiple mass movements. In these six large zones, geomorphic evidence of the presence of several landslides was found, but due to soil erosion and anthropogenic impact on local topography the delineation of all individual landslides was impossible. In total the number of landslides in the 500 km^2 study area is estimated to be at least 100. Together they cover ca. 14.8% of the study area. Some of these landslides are probably very old. Nyssen et al. (2003) assumes they initiated during the Late Pleistocene to Middle Holocene. However, we distinguished different categories of freshness of the typical morphological landslide characteristics (e.g. main scarp, reverse slope, and foot) and different stages in the evolution of the

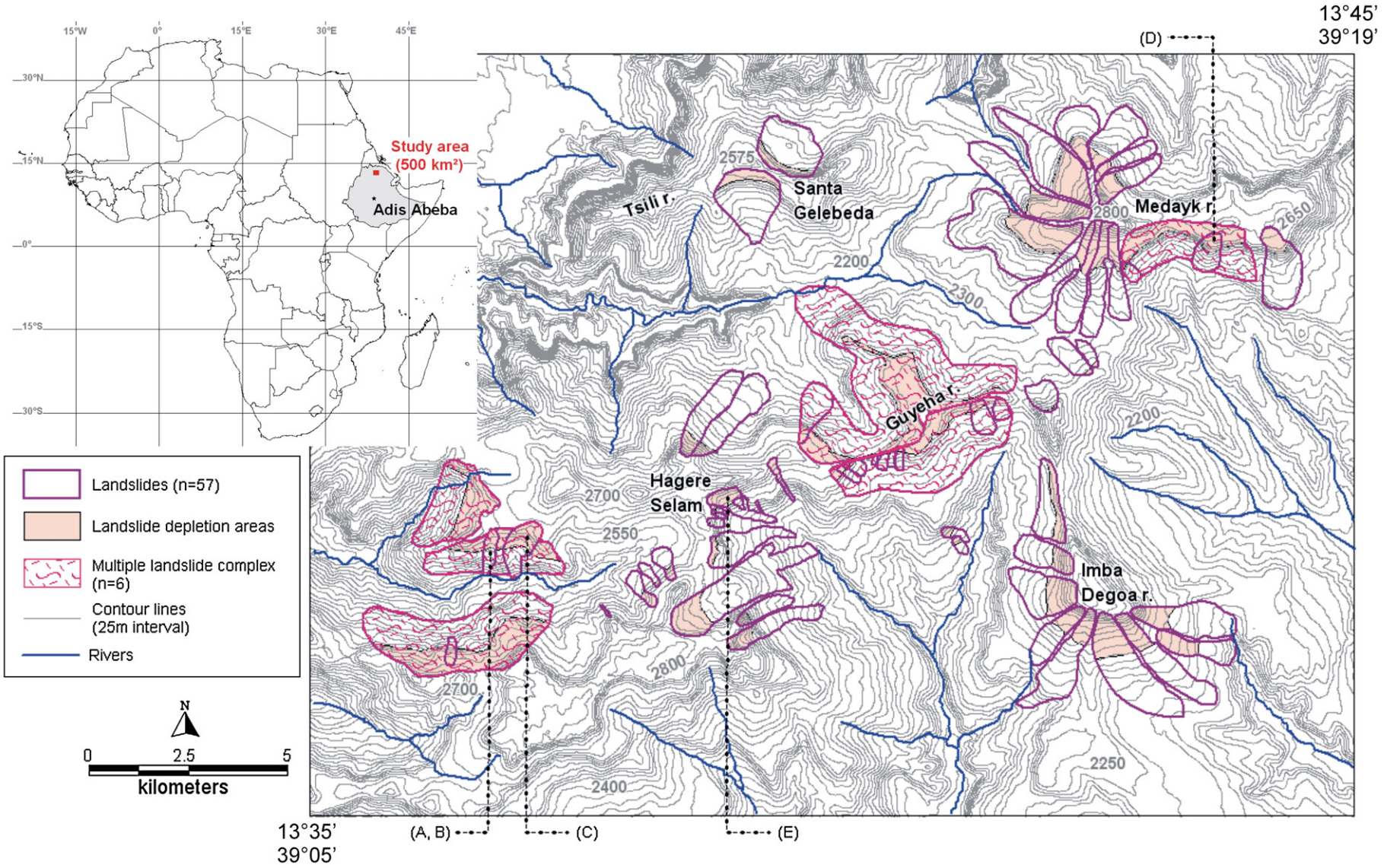

Fig. 1. Topographic contour line map of the 500 km^2 study area around Hagere Selam in Tigray, northern Ethiopia, and location of large landslides (57 complex slides and debris flows) and six zones with multiple landslides. A–E indicate location of landslides shown in Fig. 3.

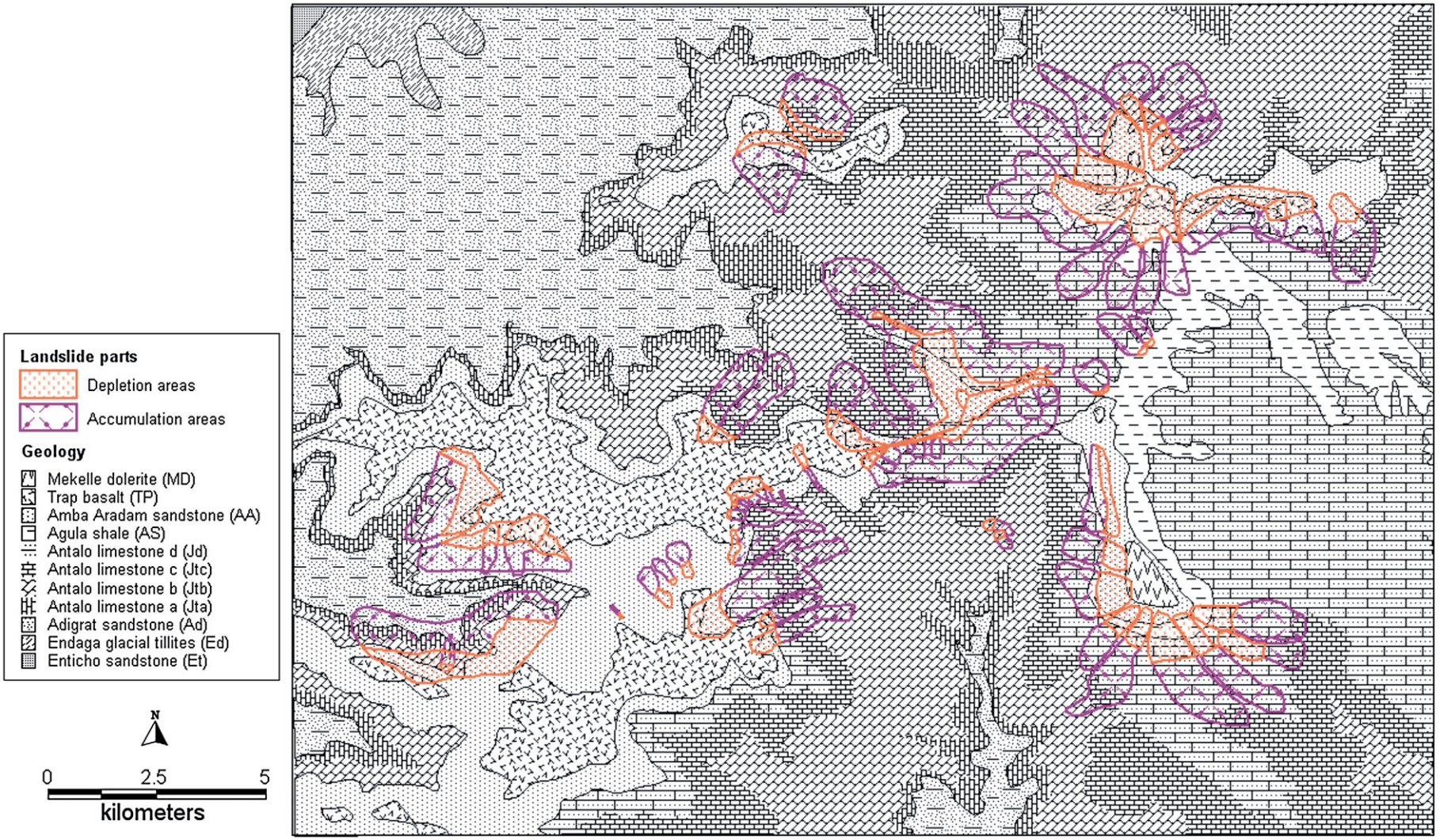

Fig. 2. Geological map of the study area (after Russo et al., 1999) with overlay of landslide depletion and landslide accumulation areas.

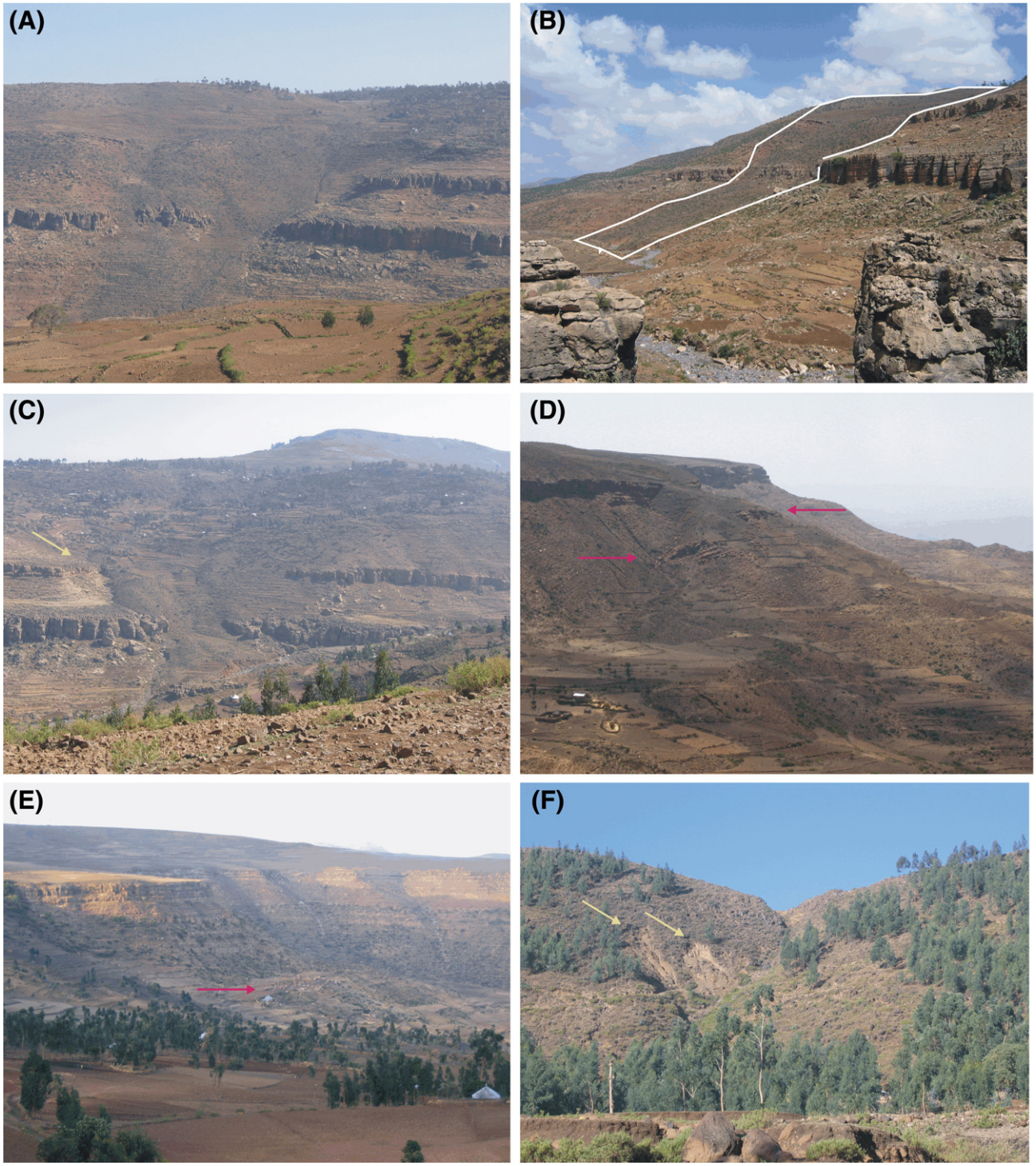

Fig. 3. Typical landslides in the study area: (A) large debris flow which initiated at the plateau border in weathered basalts and lacustrine intercalations and flowed over the Amba Aradam sandstone cliff and two underlying Antalo limestone cliffs. Note the concave depletion area, and the toppled rocks in front of the cliffs; (B) side view of debris flow shown in (A). Again the concave depletion area is clearly visible; (C) debris flow located east of the flow shown in (A). Note the settlement located in the depletion area; (D) debris flow has cut through the Amba Aradam sandstone cliff. Red arrows indicate tilted sandstone blocks that were dragged downslope by the debris. Yellow arrow indicates more recent rock fall (not included in this study); (E) rotational slide. Red arrow indicates reverse slope consisting of large blocks of Amba Aradam sandstone; (F) recent translational debris slides. Such relatively small slides were not included in this analysis (see Fig. 1 for location of landslides).

internal drainage pattern after landslide initiation. Both the observation of different phases in freshness of landslide characteristics and in internal drainage pattern (Keaton and DeGraff, 1996) indicate that landslides were initiated or reactivated during different periods in the past. Compared to Fig. 3D, C for example shows a rotational landslide with a fresher morphology. On both figures one can distinguish a clear reverse slope downslope of the main scarp, but from the landslide on Fig. 3D more hillslope material has been removed by subsequent soil erosion by water. In the field, also several small, more recent shallow debris flows and translational slides were observed (Fig. 3F). Their location was indicated on the 1:50,000 topographical map, but they were not included in this analysis, because it is not appropriate to

establish one model for different landslide types. Also rock falls are not included in this analysis, because these are very different slope processes. Cliff recession through rock fall was studied by Nyssen et al. (2006) who measured for a 1500 m long section of the Amba Aradam cliff an average annual recession of 0.37 mm. With ca. 357 km of rock cliffs higher than 10 m in the study area, the annual rock fall volume is thus estimated to be at least 1320 m^3. More information on the landslide mapping and classification can be found in Moeyersons et al. (2008).

Finally, the study area consists of 88,053 grid cells (30 m×30 m) located within a large landslide. These landslide-affected grid cells were given a value of one while a zero value was given to 505,947 grid cells located outside a landslide.

3.2. Weights of evidence and evaluation and validation of calibrated models

When sufficient data are available the relative importance of a set of controlling factors can be estimated statistically using weights of evidence modelling (WofE). This Bayesian approach in a log-linear form, and implemented in a GIS framework, has proven valuable for landslide susceptibility mapping in previous studies (e.g. Lee et al., 2002; van Westen et al., 2003; Thiery et al., 2004; Neuhäuser and Terhorst, 2007; Poli and Sterlacchini, 2007; Sharma and Kumar, 2007; Mathew et al., 2007; Dahal et al., in press).

A detailed description of the mathematical formulation of the WofE method is given in e.g. Bonham-Carter et al. (1989) and Agterberg et al. (1990), and more recently in e.g. Lee et al. (2002), van Westen et al. (2003) and Dahal et al. (in press). In short, for each category of a categorical or a classified continuous variable (X_1, …, X_k) a positive (W^+) and negative (W^-) weight are calculated based on the presence or absence of the landslides within the area. Provided that the controlling factors used as variables are conditionally independent, the posterior probability or landslide susceptibility can be estimated from these weights and the prior probability.

For derivation in a raster GIS, IDRISI Andes and using grid cells with a 30 m×30 m resolution, positive (W^+) and negative (W^-) weights can be calculated as:

$$W_i^+ = \log_e \left[\frac{\frac{N(LS/X_i)}{N(LS)}}{\frac{N\left(X_i/\overline{LS}\right)}{N\left(\overline{LS}\right)}} \right] \quad (1)$$

$$W_i^- = \log_e \left[\frac{1-\frac{N(LS/X_i)}{N(LS)}}{1-\frac{N\left(X_i/\overline{LS}\right)}{N\left(\overline{LS}\right)}} \right] \quad (2)$$

where: $N(LS/X_i)$ is the number of cells in a (mapped) landslide and with the presence of a certain category of a variable (X_i); $N(LS)$ is the number of cells in a (mapped) landslide; $N\left(X_i/\overline{LS}\right)$ is the number of cells with the presence of a certain category of a variable (X_i) and located outside of a (mapped) landslide and; $N\left(\overline{LS}\right)$ is the number of cells outside a (mapped) landslide.

In this study not all 594,000 grid cells were used, but weights were calibrated using a subsample of ca. 5000 grid cells (i.e. n=4990) taken by stratified random selection. About 15.1% (i.e. n=754) of these cells were affected by a landslide. χ^2 tests proved that this sample was representative for the total study area. A positive (negative) W_i^+ obtained for a certain category of a variable means that the presence of this category in a grid cell will (not) contribute to landslide susceptibility. Similarly, a negative (positive) W_i^- means that the absence of the category will (not) favour slope stability (van Westen et al., 2003). For each grid cell, the contrast C indicates how well a category predicts landslide occurrence incorporating both weights (Raines, 1999). C is calculated as:

$$C = W_i^+ - W_i^- \quad (3)$$

and is a first parameter that helps in distinguishing important variables from less important variables. C has a zero value when a category has no statistical relationship with the occurrence of landslides. In order to select significantly contributing variables studentized contrasts (*StudC*) were calculated as the ratio of the

Table 1
Classification of independent variables using a priori information on landslide locations to maximize contrast values, and results of WofE modelling for deep-seated landslides (see Fig. 2 for details on lithological formations)

	% landslides	% study area	W^+	W^-	C	*StudC*
Altitude (m a.s.l.)						
[1650–2294)	10.63	49.80	0.00	0.58	−0.58	−3.61**
[2294–2388)	21.67	17.27	0.23	−0.05	0.28	2.13**
[2388–466)	31.76	11.74	1.00	−0.26	1.25	9.53**
[2466–2559)	20.32	9.22	0.79	−0.13	0.92	6.42**
[2559–2850]	15.61	11.96	0.27	−0.04	0.31	2.10**
Slope (°)						
[0–5.2)	17.09	24.97	0.00	0.10	−0.10	−0.72
[5.2–8.4)	27.05	21.68	0.22	−0.07	0.29	2.35**
[8.4–12.9)	28.40	21.28	0.29	−0.09	0.38	3.10**
[12.9–20)	17.90	19.10	−0.06	0.01	−0.08	−0.58
[>20]	9.56	12.97	−0.31	0.04	−0.34	−2.05**
Aspect						
N	15.38	13.33	0.00	−0.02	0.02	0.17
NE	14.19	16.33	−0.14	0.03	−0.17	−1.13
E	10.34	12.61	−0.20	0.03	−0.22	−1.37*
SE	12.86	11.62	0.10	−0.01	0.12	0.75
S	16.18	13.41	0.19	−0.03	0.22	1.54*
SW	11.01	11.46	−0.04	0.01	−0.05	−0.28
W	9.42	10.22	−0.08	0.01	−0.09	−0.54
NW	10.61	11.02	−0.04	0.00	−0.04	−0.26
Profile curvature						
Convex	38.59	37.45	0.00	−0.02	0.02	0.16
Flat	23.34	22.99	0.02	0.00	0.02	0.16
Concave	38.06	39.56	−0.04	0.02	−0.06	−0.55
Plan curvature						
Convex	46.02	45.31	0.00	−0.01	0.01	0.12
Flat	13.40	13.25	0.01	0.00	0.01	0.09
Concave	40.58	41.44	−0.02	0.01	−0.04	−0.31
Geology						
MD	0.00	0.22	0.00	0.00	0.00	−0.06
TB	5.84	6.83	−0.16	0.01	−0.17	−0.83
AA	25.86	13.67	0.64	−0.15	0.79	6.07**
AS	4.51	3.77	0.18	−0.01	0.19	0.82
Jd	33.02	16.95	0.67	−0.22	0.88	7.17**
Jtc	9.68	12.67	−0.27	0.03	−0.30	−1.82**
Jtb	17.11	20.80	−0.20	0.05	−0.24	−1.75**
Jta	2.79	6.13	−0.79	0.04	−0.82	−3.10**
Rest	1.19	18.96	−2.77	0.20	−2.96	−7.89**
Distance to faults (m)						
[0–330)	26.24	30.30	0.00	0.06	−0.06	−0.46
[330–710)	24.09	21.04	0.14	−0.04	0.17	1.37*
[710–1130)	22.88	15.61	0.38	−0.09	0.47	3.59**
[1130–1730)	15.48	13.25	0.16	−0.03	0.18	1.25
[>1730]	11.31	19.80	−0.56	0.10	−0.66	−4.22**
Distance to downslope river (m)						
[0–98)	25.30	30.58	0.00	0.07	−0.07	−0.59
[98–214)	29.21	29.26	0.00	0.00	0.00	−0.02
[214–357)	25.03	22.89	0.09	−0.03	0.12	0.94
[>357]	20.46	17.27	0.17	−0.04	0.21	1.56*

Positive (W^+) and negative (W^-) weights, contrasts (C) and studentized contrasts (*StudC*) are obtained from a representative sample of 4990 grid cells throughout the study area. Asterisks indicate significance level (**α=0.05; * α=0.10).

contrast and the standard deviation of the contrast (Raines, 1999; Poli and Sterlacchini, 2007). *StudC* is used in a similar manner to a student *t*-test of significance of the contrast. A value of 1.28, corresponding to a confidence level of 90%, was selected for *StudC* and represents the minimum acceptable confidence threshold established for this study.

As weights are calculated with a log-linear formula, weights of categories that significantly contribute to landslide occurrence can be combined. In order to include only categories of conditionally independent variables, a pairwise test supported by the χ^2 test was performed (Lee et al., 2002; Thiery et al., 2004).

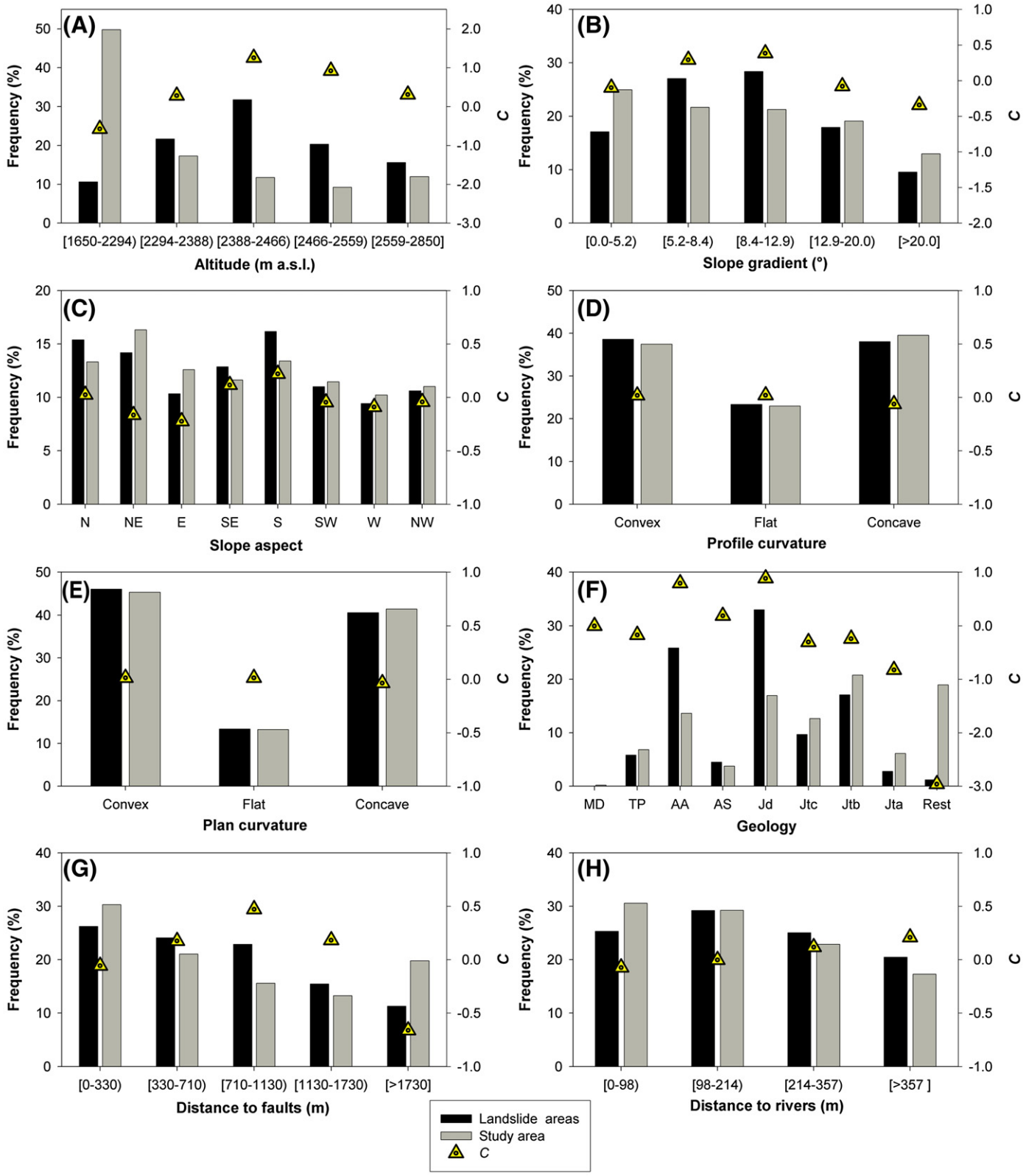

Fig. 4. Distribution of environmental variables for deep-seated landslides and for the study area as obtained from a representative sample of 4990 grid cells throughout the study area. Environmental variables are classified using a priori information on landslide locations to maximize contrast values (*C*), also shown in the histograms, obtained with WofE.

Calibrated models were evaluated with confusion matrices, Receiver Operating Characteristic curves (ROC curves, e.g. Begueria, 2006; Van Den Eeckhaut et al., 2006), success rate curves (e.g. Chung and Fabbri, 2004), Cohen's Kappa values (Cohen, 1960) and Prevalence and Bias Adjusted Kappa (Byrt et al., 1993; Van Den Eeckhaut et al., 2006) obtained for the calibration dataset of 4990 grid cells. In order to create confusion matrices or contingence matrices (e.g. Van Den Eeckhaut et al., 2006), grid cells were classified into one of the response levels (i.e. high versus low susceptibility to landslides). In this study, grid cells with a landslide probability above and below 0.5 were classified as cells susceptible or not susceptible to landsliding. Confusion matrices were created by comparing the dichotomous dependent variable (i.e. the presence or absence of a mapped landslide) with the classified model results. These matrices contain information on false positives (*FP*), false negatives (*FN*), true positives (*TP*) and true negatives (*TN*), allowing calculation of sensitivity, specificity and percentage of correctly classified observations. Sensitivity is the number of correctly predicted landslide-affected grid cells (i.e. *TP*) over the total number of mapped landslide-affected grid cells (i.e. *TP+FN*), and specificity is the number of correctly predicted landslide free grid cells (i.e. without a mapped landslide; *TN*) over the total number of mapped landslide free grid cells (i.e. *FP+TN*) (Lasko et al., 2005). A ROC curve then plots sensitivity versus 1-specificity as the cut-off value varies from 0 to 1. A model with a perfect accuracy has a ROC curve running vertically from [0,0] to [0,1] and then horizontally to [1,1], whereas the curve of a model performing no better than random guessing runs diagonally from [0,0] to [1,1] (Lasko et al., 2005). Although sensitive to prevalence (e.g. considerable difference between observed positives and observed negatives; Begueria, 2006) success rate curves (Chung and Fabbri, 2004; Guzzetti et al., 2006) were created using the calibration dataset. A success rate curve plots the proportion of the study area in each susceptibility class against the proportion of landslide area in the same class. It is no prediction rate curve (Chung and Fabbri, 2004) as for the latter the landslide data used for the confrontation with the susceptibility map may not be used for the model calibration. Hence, success rate curves evaluate calibrated models, while prediction rate curves validate calibrated models.

Cohen's Kappa index (κ) is calculated as (Cohen, 1960):

$$\kappa = \frac{P_{obs} - P_{exp}}{1 - P_{exp}} \quad (4)$$

where P_{obs} is the observed agreements; and P_{exp} is the expected agreements, which are calculated as:

$$P_{obs} = \frac{TP + TN}{N} \quad (5)$$

and

$$P_{exp} = \frac{(TP + FN)(TP + FP) + (FP + TN)(FN + TN)}{N^2} \quad (6)$$

where N is the total number of grid cells used in the analysis. κ determines the agreement between two classifications and varies from slight [<0.20), over fair [0.20–0.40), moderate [0.40–0.60), substantial [0.60–0.80) to nearly perfect [0.80–1]. Byrt et al. (1993) and Di Eugenio and Glass (2004) reported that κ are underestimated when bias (e.g. considerable difference between observed and predicted positives or observed and predicted negatives) and/or prevalence effects are present. Therefore the Prevalence and Bias Adjusted Kappa (*PABAK*; Byrt et al., 1993) was defined as:

$$PABAK = 2P_{obs} - 1 \quad (7)$$

With regard to validation of the obtained results with data not used for calibration of the weights and contrasts, temporal validation of obtained landslide susceptibility models was not possible in this study, because identified landslides could not be classified in two groups of different ages. We applied spatial validation, and evaluated obtained models using ROC and prediction rate curves and Kappa values produced for (1) a validation dataset of a second stratified random sample of ca. 5000 grid cells (i.e. 4991), and (2) all 594,000 grid cells in the study area.

3.3. Independent variables

As independent variables, topographical, lithological and hydrological characteristics were selected. Topographical factors are elevation a.s.l, hillslope gradient, slope aspect, and plan and profile curvature. All these variables were derived from SRTM (Shuttle Radar Topography Mission; http://www2.jpl.nasa.gov/srtm/cbanddataproducts.html) data using standard procedures in IDRISI Andes. Whereas the original SRTM images have a 90 m×90 m resolution, we started from a modified, 30 m×30 m resolution image (Haregeweyn, 2006). A focal mean filter was applied to fill up grid cells where the SRTM radar did not provide data due to shade effects (e.g. steep cliffs). Then contour lines with a 20 m interval were created and with TIN interpolation the 30 m×30 m resolution DEM was derived from these contour lines. Detailed cross-checks with GPS points measured throughout the study area and with the contour lines on the topographical map showed that the obtained DEM could be used in this study. As the topographical variables derived from this DEM were continuous, they had to be classified for the WofE analysis. In contrast to previous studies using WofE for landslide modelling (van Westen et al., 2003; Neuhäuser and Terhorst, 2007; Song et al., 2008; Dahal et al., in press), we followed the advice of Bonham-Carter et al. (1989) and classified the variables using a priori information on landslide presence, so that *C* values were maximized. For the classification of the continuous variables, we selected the grid cells located inside landslides from the stratified random selection of 4990 grid cells used for establishing the weights and contrasts. These 754 grid cells were classified using natural breaks. Obtained class boundaries were then used for classification of all 4990 grid cells, and weights were calculated. As weights and contrasts change with the number of categories, our method based on natural breaks was applied to segment each continuous variable in four different classifications (i.e. with three to six classes). For each variable the classification with the highest contrast and significance value were selected for the modelling. Using this approach, elevation a.s.l was subdivided in five classes between 1650 and 2850 m (Table 1). The same number of classes was chosen for hillslope gradient. Slope aspect was regarded as a categorical variable distinguishing between hillslope sections with north, northeast, east, southeast, south, southwest, west and northwest orientations. Finally, curvature in plan and profile could be concave, flat or convex.

Table 2
Results of χ^2 test for conditional independence (e.g. with α=0.05. *df*=degree of freedom, 208.9=measured χ^2, 26.3=theoretical χ^2)

Measured χ^2, (*df*/theoretical χ^2)	Elevation	Slope gradient	Aspect	Geology	Distance to faults
Slope gradient	208.9 (16/26.3)				
Aspect	115.2 (28/41.3)	147.1 (28/41.3)			
Geology	4014.6 (36/51.0)	817.8 (36/51.0)	635.2 (63/82.5)		
Distance to faults	344.9 (16/26.3)	107.5 (16/26.3)	181.3 (28/41.3)	802.2 (36/51.0)	
Distance to rivers	477.9 (12/21.0)	111.2 (12/21.0)	*24.1 (21/32.7)*	432.6 (27/40.1)	45.6 (12/21.0)

Results in italic show that slope aspect and distance to rivers are not conditional independent.

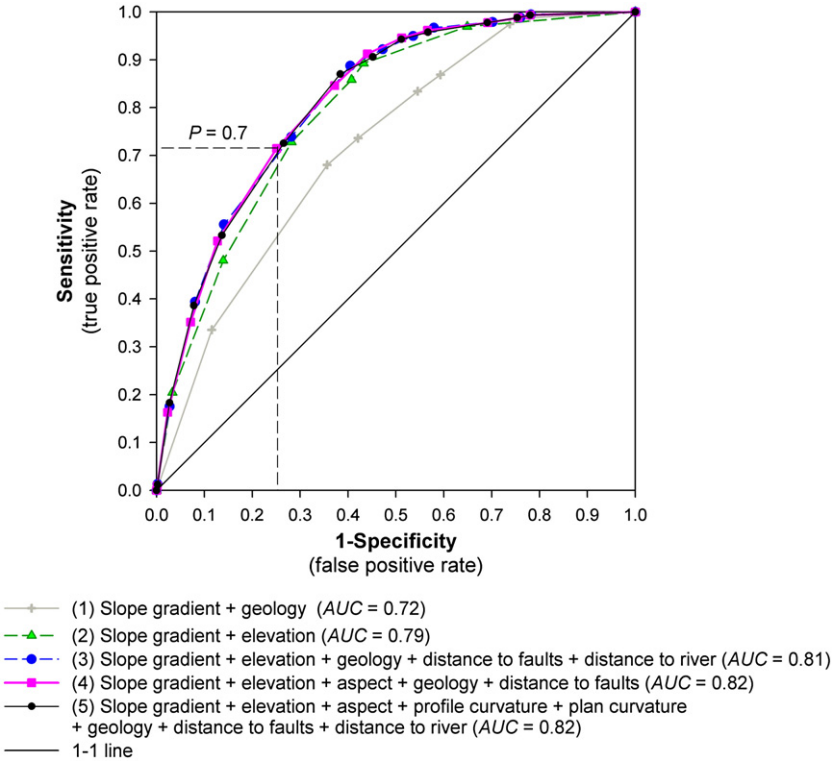

Fig. 5. ROC curves of five landslide susceptibility models resulting from WofE analysis. Hashed lines indicate that for a probability (*P*) of 0.7 model (4), selected as the best model in this study, correctly classifies 71% of the mapped landslides as landslide susceptible area (i.e. sensitivity). Approximately 25% of the area where no landslide is mapped is classified as susceptible to landslides by the model (i.e. 1-specificity).

Data on geology and faults were derived from the 1:100,000 geological map of Mekelle outlier (Russo et al., 1999). For the study area, this map shows 11 geological layers (Fig. 2), but for this study the number of classes was reduced to nine by combining the three oldest geological layers. Faults and fractures were digitized from the geological map, and distance to faults was derived in IDRISI Andes, and classified into five classes (Table 1) using natural breaks as described above. Distance to rivers was derived after digitizing the important rivers from the topographical map. The variable was classified into four classes (Table 1).

4. Results

4.1. Univariate analysis of weights and contrasts

The resulting weights and contrasts as shown in Table 1 reflect the importance of each category of the independent variables. For W^+ and *C*, positive values contribute to landslides while negative values rather indicate stable zones. For W^- it is the other way around. Table 1 shows many categories with values close to 0, meaning that they hardly show any relation with slope stability.

One or more of the categories of elevation, hillslope gradient, slope orientation, geology and distance to faults and downslope rivers have *StudC* values above 1.28 (Table 1), and hence significantly (α=0.10) influence deep-seated slope instability. Although we observed during the field checks that some landslide depletion areas are clearly located in concavities (e.g. Fig. 3A,B), neither plan nor profile curvature contributes significantly to slope instability according to the model results (Table 1; Fig. 4D,E). Positive values of *C* indicate that landslides are mainly located above ca. 2300 m a.s.l with a maximum occurrence at altitudes between ca. 2390 and 2560 m a.s.l (Fig. 4A). In contrast to most landslide studies, the deep-seated landslides are not expected to be found on the steepest hillslope sections in the study area as negative *C* values were found for hillslope sections above 20° (Table 1; Fig. 4B). Sites affected by an old deep-seated landslide, typically have slope gradients between 5° and 13°. *C* values for slope aspect suggest a higher and lower spatial occurrence of landslides on south- and east-oriented hillslopes respectively (Fig. 4C).

With regard to geology (Fig. 4F), WofE suggests that deep-seated landslide are significantly associated with the presence of Amba Aradam sandstones (AA) and upper layers of Antalo limestone (Jd). Negative *C* values indicate that older geological formations are generally not affected by landslides. Fig. 4G shows that the areal proportion of the study area decreases with distance to faults. The proportion of areas affected by landslide depletion zones is relatively constant for distances ranging between 0 and 1130 m from a fault, resulting in a significant peak in *C* values at distances between 710 and 1130 m from faults. Finally, Fig. 4H shows little variation in *C* values of downslope distance to

Table 3
Values of area under the ROC curve (*AUC*) obtained from application of the five tested models to (i) 4990 grid cells used for calibration (i.e. derivation of weights and contrasts shown in Table 1); (ii) 4991 grid cells used for validation; and (iii) all 594,000 grid cells in the study area

Models	Datasets		
	Calibration 4990 grid cells	Validation 4991 grid cells	Study area 594,000 grid cells
1) Slope gradient+geology	0.719	0.717	0.708
2) Slope gradient+elevation	0.794	0.796	0.798
3) Slope gradient+elevation+geology+distance to faults+distance to rivers	0.813	0.815	0.811
4) Slope gradient+elevation+aspect+geology+distance to faults	0.814	0.818	0.814
5) All: Slope gradient+elevation+aspect+profile curvature+plan curvature+geology+distance to faults+distance to rivers	0.814	0.816	0.812

The fourth model was finally selected, as for this model (containing conditional independent variables only) the highest *AUC* values were obtained.

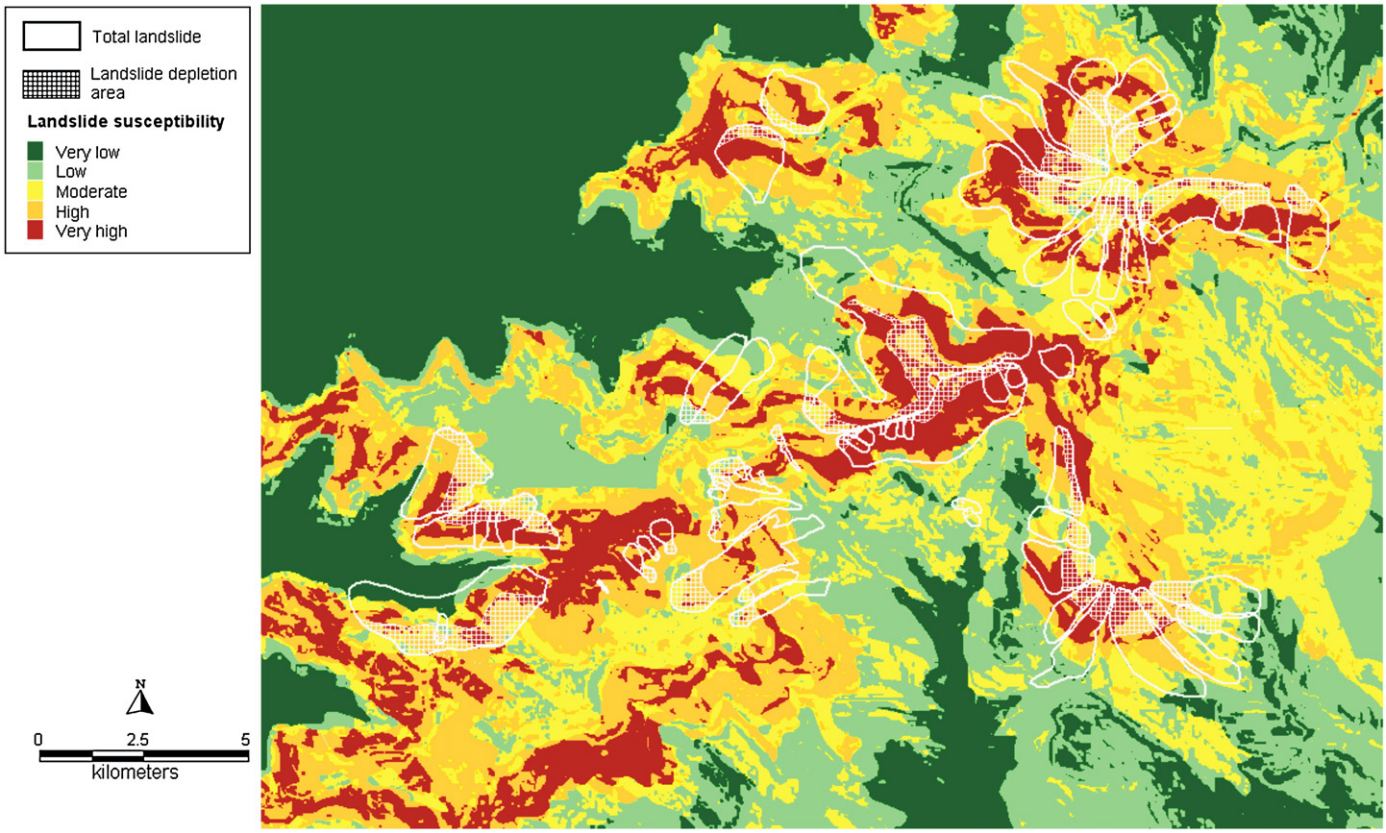

Fig. 6. Classified susceptibility map for deep-seated landslides in the study area. The map is derived with WofE using weights obtained for elevation, slope gradient, slope aspect, geology and distance to faults (i.e. model 4).

rivers. *StudC* values above 1.28, however, indicate a significant presence of landslides at distances of more than 350 m from a river.

4.2. Landslide susceptibility maps based on a combination of significant variables

Before the weights of the significant variables can be combined for estimating the posterior probability of landslide occurrence, conditional independence was tested. χ^2 analysis was used to test the conditional independence of elevation, slope gradient, slope aspect, geology, distance to faults and downslope distance to rivers. Pairwise confrontation (Table 2) learned that aspect and distance to rivers were not independent. Hence, these two variables could not be used in the same analysis. In total, posterior probability of landslide occurrence was estimated for five different models or combinations of variables:

1) a model based on slope gradient and geology as these are the most important environmental causal factors in many landslide susceptibility studies;
2) a model based on slope gradient and elevation, the two most important topographical variables;
3) a model based on slope gradient, elevation, geology, distance to faults and downslope distance to rivers, five conditionally independent variables;
4) a model based on slope gradient, elevation, aspect, geology and distance to faults, five conditionally independent variables; and
5) a model ignoring the presence of conditional independent variables, based on all eight variables (i.e. slope gradient, elevation, aspect, profile and plan curvature, geology, and distance to faults and to downslope rivers).

To evaluate and compare the five models, Fig. 5 shows the ROC curves obtained from the dataset of 4990 grid cells used for derivation of weights and contrasts (i.e. calibration). The graph shows that the curves of models 2 to 5 are similar, and have an area under the ROC curve (i.e. *AUC*) between 0.79 and 0.82. Hence, they are capable of predicting a considerable number of landslide-affected grid cells without attributing a high susceptibility to large numbers of grid cells without a mapped landslide. For a probability of 0.70, model 4 for example correctly classifies 71% of the 754 truly affected landslide grid cells (i.e. sensitivity or true positive rate; Fig. 5). About 25% of the 4236 grid cells outside a mapped landslide are false positives, i.e. classified as susceptible by the model. The term misclassified is not used here, because 1) some of these areas might have low slope stability and could be affected by a landslide under conditions similar to those that triggered the mapped landslides, or 2) some false positives might be due to mapping errors at the boundaries of the old, deep-seated landslides. For the latter we refer to Section 5 where the accuracy of the maps used will be further discussed. The ROC curve of model 1 based on slope gradient and geology is located lower in the graph (i.e. *AUC* = 0.72), reflecting that this model is less capable of explaining the occurrence of deep-seated landslides. *AUC* values were not only calculated for the calibration dataset, but also for a validation dataset of 4991 stratified randomly selected grid cells and for all 549,000 grid

Table 4
Five classes used for classification of the landslide susceptibility map shown in Fig. 6, and the distribution of mapped landslides within these classes

Susceptibility	Probability	Landslide depletion area		Landslide area	
		%	Cumulative %	%	Cumulative %
Very high	[0.85–1.00]	34.5	34.5	11.4	11.4
High	[0.70–0.85)	38.5	73.0	20.9	32.3
Moderate	[0.55–0.70)	17.8	90.8	19.2	51.5
Low	[0.30–0.55)	7.3	98.1	22.1	73.6
Very low	[0.00–0.30)	1.9	100.0	26.4	100.0

cells in the study area (Table 3). For each model, *AUC* values obtained for the three different datasets are nearly equal. This means that all five models are validated successfully as they are capable of predicting susceptibility for grid cells not used for model calibration. Finally, model 4 was selected because this was the model with the highest *AUC* values, and without dependent variables. For this model a classified landslide susceptibility map was created (Fig. 6). Class boundaries (Table 4) were chosen after evaluation of the ROC curve and of the sensitivity, specificity, correctly classified grid cells and Kappa values calculated for different probabilities (i.e. cut off values) between 0 and 1 (Fig. 7). On the classified map very high susceptibility

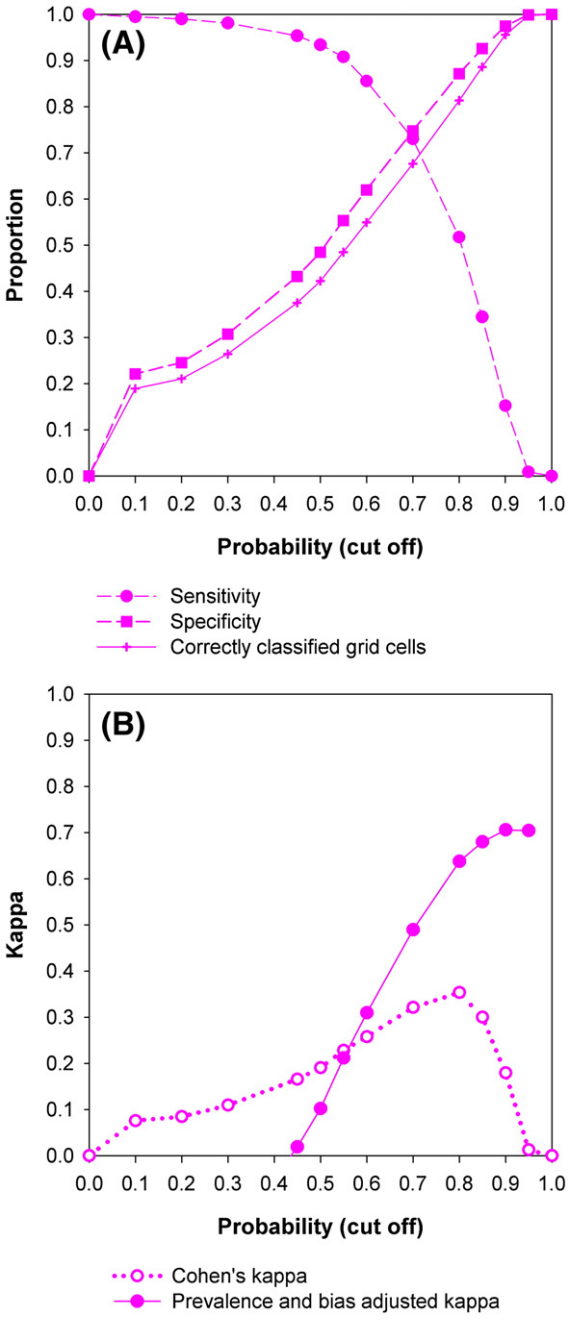

Fig. 7. Evolution of evaluation values for probability values ranging between 0 and 1 that allows derivation of meaningful classes to classify the landslide susceptibility map: (A) evolution of sensitivity, specificity and proportion of correctly classified grid cells; (B) evolution of Cohen's Kappa and Prevalence and Bias Adjusted Kappa. The parameters shown are obtained from application of model 4 to all 594,000 grid cells in the study area.

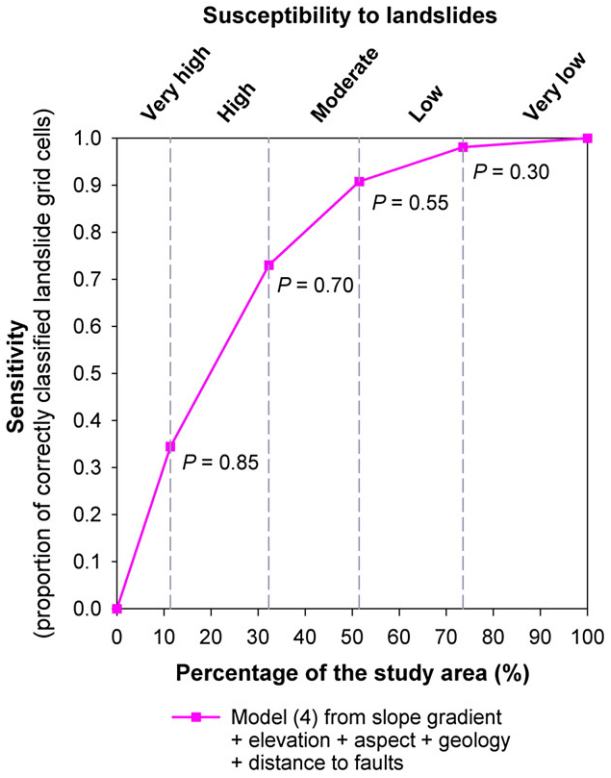

Fig. 8. Prediction rate curve obtained from application of model 4 to all 594,000 grid cells in the study area. Values were calculated for the probabilities (*P*) that were used for classifying the landslide susceptibility map into five classes (i.e. very high, high, moderate, low and very low). The proportion of the study area in each susceptibility class is indicated with hashed lines in the graph.

to deep-seated landslides was attributed to grid cells with a posterior probability above 0.85. This threshold is based on the prior probability of landslide occurrence (i.e. 0.148; Table 4). Note that *PABAK* reaches a maximum around this probability (Fig. 7B). The lower boundary of the high susceptibility class was chosen at 0.70, where sensitivity and specificity values cross when plotted against probability (Fig. 7A), or in other words, at the probability threshold resulting in the best combination of correctly classified landslide-affected grid cells and incorrectly classified grid cells without a mapped landslide. The lower boundary of the classes with moderate (i.e. probability = 0.55) and low (i.e. probability = 0.30) susceptibility are chosen because of changes in the gradient of the sensitivity and specificity curve in Figs. 5 and 7A.

In total, very high and high susceptibility classes cover 32% of the study area (Table 4), more than twice the mapped affected area (i.e. 14.8%). The overlay of the mapped landslides and the classified susceptibility map (Fig. 6) shows a rather good correspondence, and the prediction rate curve (Fig. 8) indicates that 73% of the mapped landslide areas are correctly classified as areas with very high or high susceptibility. Almost 91% of the mapped landslide areas are located in areas with very high to moderate susceptibility, comprising more or less half the study area. Hence, the model succeeds in indicating areas where deep-seated landslides are located. Only for long-runout landslides, a low susceptibility is sometimes attributed to the most downslope part of the landslide foot.

5. Discussion

When evaluating the obtained model results, it is important to take into account that the accuracy of the output is strongly depending on the quality of the input data, i.e. the landslide inventory, the SRTM images, the 1:50,000 topographical map, the aerial photographs, and the 1:100,000 geological map of the Mekelle outlier (Russo et al.,

1999). In previous studies where more detailed topographical data were not available (e.g. Neuhäuser and Terhorst, 2007), the use of SRTM images resulted in landslide susceptibility maps of acceptable quality. For this study, the improved 30 m×30 m resolution DEM derived from SRTM by Haregeweyn (2006) was chosen after critical evaluation (see Section 3.3). However, it should be taken into account that topography is smoothed on the DEM, resulting in underestimation of hillslope gradients. In contrast to LIDAR-derived topographical maps (e.g. Schulz, 2007; Van Den Eeckhaut et al., 2007), the contour line maps and hillshade maps derived from the 30 m×30 m resolution DEM were too coarse to allow a detailed delineation of deep-seated landslides in the study area. Therefore landslides were mapped from aerial photos in combination with detailed field checks by four geomorphologists experienced in landslide mapping. The experience of geomorphologists, however, cannot avoid errors at the boundaries of the old landslides, which over time became less clear by soil erosion due to water and tillage and by human interventions such as agricultural activities, and levelling for construction of roads and houses. But the effect of incorrect delineations of landslide boundaries will be limited in our WofE analysis, as weights and contrasts are calculated from a confrontation of a representative sample of grid cells located outside and inside (i.e. not at the boundaries) of mapped landslides with classified maps of the independent variables. With regard to the lithological map, small lithological errors (i.e. incorrect indication of local lithology, or local errors in geometric rectification) were detected during the field visits. Given that only local corrections could be made, we decided to use the map published by Russo et al. (1999). The fault map (Russo et al., 1999) shows faults and fractures that were visible on aerial photographs. The location of mapped faults is relatively accurate, but nothing is known about the completeness of the map. Finally the major and moderate-sized rivers, digitized from the topographical map, were correctly located in the valleys present on the SRTM-derived contour line maps. Hence, the variable downslope distance to rivers has an accuracy similar to the other topographical variables.

Although it is important to be aware of abovementioned possible mapping errors, a critical analysis of the weights and contrasts, ROC curves and success and prediction rate curves allows us to conclude that for the 500 km^2 study area, WofE enabled the production of a landslide susceptibility map showing the propensity to be affected by deep-seated landsliding. The quality of the map (Fig. 6) was successfully tested by calibrating five models for a stratified random sample of 4990 grid cells, and validating these models in 4991 other randomly chosen grid cells and in the complete study area.

The results of WofE contribute to the understanding of spatial patterns of deep-seated landslides in the study area, as they provide information on the importance of both environmental causal factors and categories within these factors. As elevation, slope gradient and lithology have most categories significant at a level of 0.05 (i.e. $StudC > 1.64$) they are regarded as the main variables explaining the spatial occurrence of the landslides. Weights obtained for these three variables learn that deep-seated landslides are mainly found on the 50% highest elevations of the study area (Fig. 4A), i.e. above 2300 m a.s.l., on slope sections with a moderate slope gradient between 5° and 13° and with Amba Aradam sandstone or Upper Antalo limestone formations. Also the variable distance to faults has significant categories. More specifically, a positive agreement between landslides and faults at distances between 710 and 1130 m were obtained. Hence, landslides are generally not located in zones with weaker lithology along faults. The variable distance to faults was also included in the analysis as deep-seated landslides in the study area might be triggered by earthquakes, but the results obtained do not allow drawing conclusions here. Finally, it is important that the results obtained for distance to downslope rivers indicate that the displaced material generally does not reach the river valley. Hence, undercutting of the slope by a river was probably not the main triggering factor of the deep-seated landslides.

The obtained findings partly confirm the initiation conditions we suggested after field observations (Moeyersons et al., 2008). Our hypothesis is that landslides were initiated on the highest plateau, above the Amba Aradam sandstone cliff, where weathering of trap basalts and intercalated lacustrine deposits resulted in the development of Vertisols and vertic Cambisols rich in smectite clays (Nyssen et al., 2008), and hillslope gradients are generally below 15°. Although little is known about the triggering factors of the old landslides (Nyssen et al., 2003), mobilisation of the weathered basalt material rich in swelling clays is believed to be driven by increased pore water pressures on the impermeable baked upper boundary of the Amba Aradam cliff. Although, similar to all lithological layers, this cliff is indicated as a nearly horizontal layer on the geological map, observations at landslide sites showed that the Amba Aradam upper boundary can be undulated, forming a depression. Probably infiltrating rain water was concentrated in these depressions, decreasing the local slope stability more compared to locations further away. The debris mobilised by the landslide was then suggested to be transported over cliffs of the Amba Aradam sandstone and Antalo limestone formations (Fig. 3A–C) and deposited on Agula shales and Antalo limestones. In the case of rotational flowing and sliding, sometimes large sandstone or limestone blocks dragged by the debris, formed reverse slopes. Hence, in this hypothesis, lithology with the presence of swelling clays and alternations of aquifers and aquitards is probably a more important causal factor than slope gradient.

WofE confirms the presence of landslides in Amba Aradam sandstones and upper Antalo limestone formations, but no association was found between landslides and trap basalts. Two reasons can be put forward. First, there is the fact that complete landslides were incorporated in this analysis. The landslide depletion areas (Fig. 1), however, comprise only 28.1% of the total landslide areas. Thus, lithologies that are more abundant in the total landslide areas have higher weights than the basalts. Secondly, and more important, is that we focus on old deep-seated landslides, and that currently all basalt might have been removed by slope processes, such as landsliding and soil erosion by water from some plateaus (e.g. Guyena ridge and Medayk ridge; Fig. 1). The presence of basaltic material downslope of the Amba Aradam sandstone cliff, on locations where nowadays no basalt is present upslope of the cliff, confirms that this explanation is valid for at least certain sites. Moreover, most landslide accumulation areas have dark soils typical for weathered basalt, which proofs that the in-situ sandstone and limestone are covered with debris. In this way the region benefits from the presence of deep-seated landslides, as the soil fertility in the accumulation area is higher than the fertility of soils developed in limestone (Moeyersons et al., 2008). Farmers in the area are aware of this higher soil fertility. In case of rotational landslides, for example, houses have been built on the Amba Aradam sandstone reverse slopes, while the surrounding fertile landslide debris is intensively cropped.

In other landslide susceptibility studies, elevation a.s.l. is not always included as independent variable, because often this variable is associated with landslides by virtue of other factors such as slope gradient, geology, precipitation or land use. In this study, elevation a.s.l. is included as no significant dependence with geology or slope gradient was found. Elevation a.s.l. is also no substitute for rainfall depth as Nyssen et al. (2003) reported that rainfall depth was controlled by slope aspect and slope gradient, but not by altitude.

The landslide susceptibility map and the results obtained not only help in understanding the location of deep-seated landslides and their impact on the geomorphological evolution of the study area. Although we acknowledge that, due to differences in environmental conditions, the susceptibility map derived for old deep-seated landslides does not directly show locations of future landslide reactivations or shallow landslide initiations, we believe that the map indirectly shows zones susceptible to landslide reactivation or initiation because studies in other parts of the world, and observations in the study area (see Section 3.1) have proven that new landslides preferentially occur on

locations already affected by landslides in the past. The maps should therefore be used as a tool for delineating inherent unstable areas where human interventions decreasing slope stability should be limited as they might induce slope failure. The examples of recent landslide activity in the Hagere Selam region, described by Nyssen et al. (2003; e.g. removal of lateral support for road construction), and the damage reported to a newly installed electricity network proof the need for such a mitigation tool. So far, it is not clear to what extent the increase in infiltration capacity of soils in areas with water conservation measures and in areas recently converted to exclosures with a rapid regeneration of natural vegetation, can contribute to landslide reactivation. If they have a strong effect on slope instability, it will be a challenge to find an equilibrium between slope stabilising measures and soil conservation measures decreasing the factor of safety in an area susceptible to both landslides and soil degradation, and most important in an area where ca. 80% of the people are still living from rain-fed agriculture (CIA World Fact Book, 2008).

6. Conclusions

For long time, the presence of old landslide bodies in a 500 km^2 study area around Hagere Selam (northern Ethiopia) was unknown. Although susceptible to soil erosion by water and tillage practices, the hillslopes were believed to be relatively stable with regard to landsliding. However, recent land use changes and human interventions have locally decreased slope stability, and old landslides were reactivated or new landslides occurred. We created a landslide inventory of the study area showing the location of 57 old landslides and six multiple landslide zones, together covering almost 14.8% of the study area. We then applied a statistical technique, WofE modelling to produce a landslide susceptibility map for the region. For the classification of the susceptibility maps, a five-category classification system chosen after analysis of sensitivity, specificity and Kappa values was adopted, and a high quality tool for explaining the spatial occurrence of the deep-seated landslides was obtained. This classification procedure is recommended to all probabilistic studies in regions with important spatial occurrence of landslides. As complete evaluation of the landslide susceptibility map requires model validation with data that was not used for the model calibration, a stratified random sample of 4990 grid cells was used for calibration of weights and contrasts. Application of the weights to a validation dataset of 4991 grid cells and to all 549,000 grid cells in the study area allowed spatial validation of the WofE results. Our results confirm that confusion matrices and ROC curves are appropriate tools for evaluation of landslide susceptibility models obtained with WofE. Although susceptible to prevalence, success and prediction rate curves also helped evaluating the results.

In the study area, deep-seated landslides are expected to be found at the border of the highest plateaus at altitudes above 2300 m on slope sections with slope gradients between 5° and 13°. The landslide debris is found on Amba Aradam sandstones and upper Antalo limestones. Initiation is hypothesized to be enhanced by the presence of white clays and marls from the lacustrine layers deposited between the trap basalts. When the volume of mobilised soil is considerable, the landslide debris will be transported over cliffs of the Amba Aradam sandstone and the Antalo limestone formations, eventually dragging large blocks of sand- and limestone, and the fertile debris (weathered basalt) will be deposited on Agula shales and Antalo limestones. Field observations indicate that Vertisols and vertic Cambisols, typical weathering products of basalt, are nowadays covering the sand- and limestone in most landslide accumulation areas. Although the created landslide susceptibility model provides no information on the triggering factors, the deep-seated landslides are believed to be driven by increasing pore water pressures (induced by high rainfall or by land use changes) in the weathered basalts resting on the impermeable Amba Aradam sandstone cliff with the baked contact.

WofE might seem inferior to other statistical models such as logistic regression or discriminant analysis, but previous studies have proven its usefulness in industrialised countries such as Germany (Neuhäuser and Terhorst, 2007), France (Thiery et al., 2004) and Italy (van Westen et al., 2003; Poli and Sterlacchini, 2007). This study demonstrates that also in regions with less detailed information on environmental characteristics the applied technique allows understanding both the distribution of old, deep-seated landslides and the present-day geomorphological characteristics of an area. We also suggest that, given that future landslides often occur on hillslopes affected by landslides in the past, the susceptibility map indirectly allows delineating zones susceptible to future slope failure. Therefore, the applied methodology can be recommended as a tool for landslide susceptibility assessment.

Acknowledgements

This research was supported by the VLIR – IUC-Mekelle 'Land Management' and 'Hydro-geology' projects. The authors thank all the staff from Mekelle University for their support and hospitality. We are also grateful to two anonymous reviewers and to Professor Oguchi for their help during the review process.

References

Agterberg, F.P., Bonham-Carter, G.F., Wright, D.F., 1990. Statistical pattern integration for mineral exploration. In: Gaal, G., Merriam, D.F. (Eds.), Computer Applications in Resource Estimation Prediction and Assessment for Metals and Petroleum. Pergamon Press, Oxford, p. 19.

Alcántara-Ayala, I., 2002. Geomorphology, natural hazards, vulnerability and prevention of natural disasters in developing countries. Geomorphology 47, 107–124.

Almond, D.C., 1986. The relation of Mesozoic Cainozoic volcanism to tectonics in the Afro-Arabian dome. Journal of Volcanology and Geothermal Research 28, 225–246.

Asrat, A., 2002. The rock-hewn churches of Tigray, northern Ethiopia: a geological perspective. Geoarchaeology 17, 649–663.

Ayalew, L., Yamagishi, H., 2004. Slope failures in the Blue Nile basin, as seen from landscape evolution perspective. Geomorphology 57, 95–116.

Ayonghe, S.N., Mafany, G.T., Ntasin, E., Samalang, P., 1999. Seismically activated swarm of landslides, tension cracks, and a rockfall after heavy rainfall in Bafaka, Cameroon. Natural Hazards 19, 13–27.

Ayonghe, S.N., Ntasin, E.B., Samalang, P., Suh, C.E., 2004. The June 27, 2001 landslide on volcanic cones in Limbe, Mount Cameroon, West Africa. Journal of African Earth Sciences 39, 435–439.

Begueria, S., 2006. Validation and evaluation of predictive models in hazard assessment and risk management. Natural Hazards 37, 315–329.

Bell, F.G., Maud, R.R., 2000. Landslides associated with the colluvial soils overlying the Natal Group in the greater Durban region of Natal, South Africa. Environmental Geology 39, 1029–1038.

Bonham-Carter, G.F., Agterberg, F.P., Wright, D.F., 1989. Weights of evidence modelling: a new approach to mapping mineral potential. In: Agterberg, F.P., Bonham-Carter, G.F. (Eds.), Statistical Applications in the Earth Sciences. Geological Survey of Canada, Ottawa, Ontario, pp. 171–183.

Bosellini, A., Russo, A., Fantozzi, P.L., Assefa, G., Solomon, T., 1997. The Mesozoic succession of the Mekelle Outlier. Memorize di scienze geologiche 49, 95–116.

Byrt, T., Bishop, L., Carlin, J.B., 1993. Bias, prevalence and kappa. Journal of Clinical Epidemiology 46, 423–429.

Carrara, A., Cardinali, M., Guzzetti, F., Reichenbach, P., 1995. GIS technology in mapping landslide hazard. In: Carrara, A., Guzzetti, F. (Eds.), Geographical Information Systems in Assessing Natural Hazards. Kluwer Acad. Publ., Dordrecht, pp. 135–176.

Chung, C.F., Fabbri, A.G., 2004. Validation of spatial prediction models for landslide hazard mapping. Natural Hazards 30, 451–472.

CIA World Fact Book (2008; https://www.cia.gov/library/publications/the-world-fact-book/index.html).

Claessens, L., Knapen, A., Kitutu, M.G., Poesen, J., Deckers, J.A., 2007. Modelling landslide hazard, soil redistribution and sediment yield of landslides on the Ugandan footslopes of Mount Elgon. Geomorphology 90, 23–35.

Cohen, J.A., 1960. A coefficient of agreement for nominal scales. Educational and Psychological Measurement 20, 37–46.

Cruden, D.M., Varnes, D.J., 1996. Landslide types and processes. In: Turner, A.K., Schuster, R.L. (Eds.), Special Report 247: Landslides, Investigation and Mitigation, Transportation Research Board. National Research Council. National Academy Press, Washington, DC, pp. 36–71.

Dahal, R.K., Hasegawa, S., Nonomura, A., Yamaka, M., Dhakal, S., Paudyal, P., in press. Predictive modelling of rainfall-induced landslide hazard in the Lesser Himalaya of Nepal based on weights-of-evidence. Geomorphology.

Davies, T.C., 1996. Landslide research in Kenya. Journal of African Earth Sciences 23, 541–545.

Descheemaeker, K., Nyssen, J., Rossi, J., Poesen, J., Haile, M., Raes, D., Muys, B., Moeyersons, J., Deckers, J., 2006. Sediment deposition and pedogenesis in exclosures in the Tigray highlands, Ethiopia. Geoderma 132, 291–314.

Di Eugenio, B., Glass, M., 2004. Squibs and discussions The Kappa Statistic: a second look. Computational Linguistics 30, 95–101.
Dramis, F., Coltorti, M., Pieruccini, P., 2002. Geological and geomorphological framework of the excursion area. In: Dramis, F., Molion, P., Cipolloni, C., Fubelli, G. (Eds.), International Symposium Addis Abbeba, 9–10 December 2002. Proceedings IAG International Symposium, pp. 1–12.
Frattini, P., Crosta, G.B., Fusi, N., Dal Negro, P., 2004. Shallow landslides in pyroclastic soils: a distributed modelling approach for hazard assessment. Engineering Geology 73, 277–295.
Garland, G.G., Olivier, M.J., 1993. Predicting landslides from rainfall in a humid, subtropical region. Geomorphology 8, 165–173.
Gebremichael, D., Nyssen, J., Poesen, J., Deckers, J., Haile, M., Govers, G., Moeyersons, J., 2005. Effectiveness of stone bunds in controlling soil erosion on cropland in the Tigray Highlands, northern Ethiopia. Soil Use and Management 21, 287–297.
Guzzetti, F., Carrara, A., Cardinali, M., Reichenbach, P., 1999. Landslide hazard evaluation: a review of current techniques and their application in a multi-scale study, Central Italy. Geomorphology 31, 181–216.
Guzzetti, F., Reichenbach, P., Ardizzone, F., Cardinali, M., Galli, M., 2006. Estimating the quality of landslide susceptibility models. Geomorphology 81, 166–184.
Haregeweyn, N., 2006. Reservoir sedimentation in the North Ethiopian Highlands: assessment and modelling of controlling factors and impacts. Ph.D. Thesis, Faculty of Science, Department of Geography, K.U. Leuven, Belgium.
Ibe, K.M., Ebe, A.M., 2000. Impacts of debris-flow deposits on hydrogeochemical processes and the development of dryland salinity in the Cross-River catchment, SE, Nigeria. Environmental Monitoring and Assessment 64, 449–456.
Keaton, J.R., DeGraff, J.V., 1996. Surface observation and geologic mapping. In: Turner, A.K., Schuster, R.L. (Eds.), Landslides, investigation and mitigation, transportation research board. National Research Council, Special Report 247. National Academy Press, Washington, DC, pp. 128–230.
Knapen, A., Kitutu, M.G., Poesen, J., Breugelmans, W., Deckers, J., Muwanga, A., 2006. Landslides in a densely populated county at the footslopes of Mount Elgon (Uganda): Characteristics and causal factors. Geomorphology 73, 149–165.
Lasko, T.A., Bhagwat, J.G., Zou, K.H., Ohno-Machado, L., 2005. The use of receiver operating characteristic curves in biomedical informatics. Journal of Biomedical Informatics 38, 404–415.
Lee, S., Choi, J., Min, K., 2002. Landslide susceptibility analysis and verification using the Bayesian probability model. Environmental Geology 43, 120–131.
Mathew, J., Jha, V.K., Rawat, G.S., 2007. Weights of evidence modelling for landslide hazard zonation in part of Bhagirathi valley, Uttarakhand. Current Science 92, 628–638.
Moeyersons, J., 1981. Slumping and planar sliding on hillslopes in Rwanda. Earth Surface Processes and Landforms 6, 265–274.
Moeyersons, J., 1989. A possible causal relationship between creep and sliding on Rwaza Hill, southern Rwanda. Earth Surface Processes and Landforms 14, 597–614.
Moeyersons, J., 2001. The palaeoenvironmental significance of Late Pleistocene and Holocene creep and other geomorphic processes, Butare, Rwanda. Palaeoecology of Africa and Surrounding Islands 27, 37–50.
Moeyersons, J., 2003. The topographic thresholds of hillslope incisions in south-western Rwanda. Catena 50, 381–400.
Moeyersons, J., Tréfois, P.h., Lavreau, J., Alimasi, D., Badriyo, I., Mitima, B., Mundala, M., Munganga, D.O., Nahimana, L., 2004. A geomorphological assessment of landslide origin at Bukavu, Democratic Republic of the Congo. Engineering Geology 72, 73–87.
Moeyersons, J., Van Den Eeckhaut, M., Nyssen, J., Gebreyohannes, Tesfamichael, Van de Wauw, J., Hofmeister, J., Poesen, J., Deckers, J., Haile, M., 2008. Mass movement mapping for geomorphological understanding and sustainable development. Tigray, Ethiopia. Catena. 75, 45–54.
Neuhäuser, B., Terhorst, B., 2007. Landslide susceptibility assessment using "weights of evidence" applied to a study area at the Jurassic escarpment (SW-Germany). Geomorphology 86, 12–24.
Ngecu, W.M., Ichang'I, D.W., 1999. The environmental impact of landslides on the population living on the eastern footslopes of the Aberdare ranges in Kenya: a case study of Maringa Village landslide. Environmental Geology 38, 259–264.
Ngecu, W.M., Mathu, E.M., 1999. The El-Nino-triggered landslides and their socio-economic impact on Kenya. Environmental Geology 38, 277–284.
Ngecu, W.M., Nyamai, C.M., Erima, G., 2004. The extent and significance of mass-movements in Eastern Africa: case studies of some major landslides in Uganda and Kenya. Environmental Geology 46, 1123–1133.
Nyssen, J., Poesen, J., Haile, M., Moeyersons, J., Deckers, J., 2000. Tillage erosion on slopes with soil conservation structures in the Ethiopian highlands. Soil and Tillage Research 57, 115–127.
Nyssen, J., Moeyersons, J., Poesen, J., Deckers, J., Haile, M., 2003. The environmental significance of the remobilization of ancient mass movements in the Atbara-Tekeze headwaters, northern Ethiopia. Geomorphology 49, 303–322.
Nyssen, J., Poesen, J., Moeyersons, J., Deckers, J., Haile, M., Lang, A., 2004. Human impact on the environment in the Ethiopian and Eritrean highlands – a state of the art. Earth Science Reviews 64, 273–320.
Nyssen, J., Vandenreyken, H., Poesen, J., Moeyersons, J., Deckers, J., Haile, M., Salles, C., Govers, G., 2005. Rainfall erosivity and variability in the northern Ethiopian Highlands. Journal of Hydrology 311, 172–187.
Nyssen, J., Poesen, J., Moeyersons, J., Deckers, J., Haile, M., 2006. Processes and rates of rock fragment displacement on cliffs and scree slopes in an amba landscape, Ethiopia. Geomorphology 81, 265–275.
Nyssen, J., Naudts, J., De Geyndt, K., Haile, M., Poesen, J., Moeyersons, J., Deckers, J., 2008. Soils and land use in the Tigray highlands (Northern Ethiopia). Land Degradation and Development 19, 257–274.
Petley, D.N., 2008. The global occurrence of fatal landslides in 2007. Proceeding of the "First World Landslide Forum Satellite Conference". Sendai, Miyagi Prefecture, Japan, p. 11.
Poli, S., Sterlacchini, S., 2007. Landslide representation strategies in susceptibility studies using weights-of-evidence modeling technique. Natural Resources Research 16, 121–134.
Raines, G.L., 1999. Evaluation of weights of evidence to predict epithermal-gold deposits in the great basin of the western United States. Natural Resources Research 8, 257–276.
Russo, A., Fantozzi, P., Tadesse, Solomon, 1999. Geological map of Mekelle Outlier (Western Sheet), 1:100 000. Cooperazione Italian Addis Ababa University.
Schulz, W.H., 2007. Landslide susceptibility revealed by LIDAR imagery and historical records, Seattle, Washington. Engineering Geology 89, 67–87.
Sharma, M., Kumar, R., 2007. GIS-based landslide hazard zonation: a case study from the Parwanoo area, Lesser and Outer Himalaya, H.P., India. Bulletin of Engineering Geology and the Environment 27, 129–137.
Soeters, R., van Westen, C.J., 1996. Slope stability recognition analysis and zonation. In: Turner, A.K., Schuster, R.L. (Eds.), Landslides: Investigation and Mitigation. Transportation Research Board Special Report, vol. 247. National Academy Press, Washington D.C., pp. 129–177.
Song, R.H., Daimaru, H., Abe, K., Kurosawa, U., Matsuura, S., 2008. Modeling the potential distribution of shallow-seated landslides using the weights of evidence method and a logistic regression model: a case study of the Sabae Area, Japan. International Journal of Sediment Research 23, 106–118.
Temesgen, B., Mohammed, M.U., Korme, T., 2001. Natural hazard assessment using GIS and remote sensing methods, with particular reference to the landslides in the Wondogenet area, Ethiopia. Physics and Chemistry of the Earth. Part C: Solar-Terrestrial and Planetary Science 26, 665–675.
Temple, P.H., Rapp, A., 1972. Landslides in the Mgeta Western Uluguru Mountains Tanzania. Geografiska Annaler 54, 157–193.
Thiery, Y., Sterlacchini, S., Malet, J.P., Puissant, A., Remaître, A., Maquaire, O., 2004. Strategy to reduce subjectivity in landslide susceptibility zonation by GIS in complex mountainous environments. "7th AGILE Conference on Geographic Information Science" Parallel Session 7.3- "Decision Support Systems/Risk Management II". Heraklion, Greece.
Van Den Eeckhaut, M., Vanwalleghem, T., Poesen, J., Govers, G., Verstraeten, G., Vandekerckhove, L., 2006. Prediction of landslide susceptibility using rare events logistic regression: a case-study in the Flemish Ardennes (Belgium). Geomorphology 76, 392–410.
Van Den Eeckhaut, M., Poesen, J., Verstraeten, G., Vanacker, V., Nyssen, J., Moeyersons, J., Van Beek, L.P.H., Vandekerckhove, L., 2007. The use of LIDAR-derived images for mapping old landslides under forest. Earth Surface Processes and Landforms 32, 754–769.
van Westen, C.J., Van Duren, I., Kruse, H.M.G., Terlien, M.T.J., 1993. GISSIZ: training package for Geographic Information Systems in Slope Instability Zonation. ITC-Publication Number 15. Theory, vol. 1. The Netherlands, ITC, Enschede, p. 245.
van Westen, C.J., Rengers, N., Soeters, R., 2003. Use of geomorphological information in indirect landslide susceptibility assessment. Natural Hazards 30, 399–419.
Zogning, A., Ngouanet, C., Tiafack, O., 2007. The catastrophic geomorphological processes in humid tropical Africa: a case study of the recent landslide disasters in Cameroon. Sedimentary Geology 199, 13–27.